1-1-2010

Reduced Electronic Spaces for Modeling Donor/Acceptor Interactions

Robert J. Cave
Harvey Mudd College

Stephen T. Edwards '06
Harvey Mudd College

John A, Kouzelos '07
Harvey Mudd College

Marshall D. Newton
Brookhaven National Laboratory

Reduced Electronic Spaces for Modeling Donor/Acceptor Interactions†

Robert J. Cave,* Stephen T. Edwards,§ and J. Andrew Kouzelos⊥

Department of Chemistry, Harvey Mudd College, Claremont, California 91711

Marshall D. Newton*

Department of Chemistry, Brookhaven National Laboratory, Upton, New York 11973

Received: March 15, 2010; Revised Manuscript Received: June 17, 2010

Diabatic states for donor (D) and acceptor (A) interactions in electron transfer (ET) processes are formulated and evaluated, along with coupling elements (H_{DA}) and effective D/A separation distances (r_{DA}), for reduced electronic spaces of variable size, using the generalized Mulliken Hush model (GMH), applicable to an arbitrary state space and nuclear configuration, and encompassing Robin−Day class III and as well as class II situations. Once the electronic state space is selected (a set of $n \geq 2$ adiabatic states approximated by an orbital space based on an effective 1-electron (1-e) Hamiltonian), the charge-localized GMH diabatic states are obtained as the eigenstates of the dipole moment operator, with rotations to yield locally adiabatic states for sites with multiple states. The 1-e states and energies are expressed in terms of Kohn−Sham orbitals and orbital energies. Addressing questions as to whether the estimate of H_{DA} "improves" as one increases n, and in what sense the GMH approach "converges" with n, we carry out calculations for three mixed-valence binuclear Ru complexes, from which we conclude that the 2-state (2-st) model gives the most appropriate estimate of the *effective* coupling, similar (to within a rms deviation of ≤15%) to coupling elements obtained by superexchange correction of H_{DA} values based on larger spaces ($n = 3-6$), and thus yielding a quasi-invariant value for H_{DA} over the range explored in the calculations ($n = 2-6$). An analysis of the coupling and associated D and A states shows that the 2-st coupling involves crucial mixing with intervening bridge states (D and A "tails"), while increasingly larger state spaces for the same system yield increasingly more localized D and A states (and weaker coupling), with H_{DA} tending to approach the limit of "bare" or "through space" coupling. These results help to reconcile seemingly contradictory assertions in the recent literature regarding the proper role of multistate frameworks in the formulation of coupling for both intra- and intermolecular ET systems.The present results are compared in detail with other reported results.

I. Introduction

Electron transfer (ET) between molecular donor (D) and acceptor (A) sites ($DA \rightarrow D^+A^-$) is typically treated in a two-state (2-st) framework, in which the transferring electronic charge (electron (e) or hole (h)) is primarily localized, respectively, on a D site (initial state) or an A site (final state). Such 2-st models have been employed in analyzing a wide range of intramolecular and bimolecular ET processes, including thermal (ground state or photoinitiated) and optical charge separation (CS), charge recombination (CR), and charge shift (CSh).[1−15] In all these cases, a key quantity governing the ET is the effective 2-st Hamiltonian matrix element, H_{DA},[12,13] a central focus of the present study, which deals with ET of the CSh type.

Although the two-state approximation (TSA) may be adequate if the two states are sufficiently separated energetically from other solute states,[16] it has frequently been noted that a larger set of electronic states may be necessary, especially when molecular spacers with low-lying states are interposed between D and A sites (as in bridge-mediated (DBA) intramolecular ET)[17−23] or when more than one state on a given D or A site must be considered (e.g., a ground (G) and locally excited (LE) state, D* or A*).[24,25] For example, in a 3-state $DA/D^*A/D^+A^-$ system, one may attempt to model the various ET processes—for example, an optical CS one ($DA \rightarrow D^+A^-$, the Mulliken charge transfer (CT) transition[26]), or the radiative recombination process (CR)), or the photoinitiated CS one ($D^*A \rightarrow D^+A^-$, which may involve exciplex formation)[27])—using the appropriate 2-st models in a pairwise fashion. However, if the states interact strongly with each other, a 3-state treatment may be required, especially in the case of radiative CR, which may involve significant intensity borrowing or other types of vibronic coupling.[28−30]

Some studies have reported calculation of effective H_{DA} values for an electronic state space of variable size, n (i.e., with $n \geq 2$), and indeed, sensitivity of H_{DA} with respect to n has been found[18−21,25,28,29,31] (in the following, n-st denotes an n-dimensional model). These results invite a closer look at the nature of the n-st variation of H_{DA} (denoted $H_{DA}^{d(n)}$) and the corresponding diabatic states in which they are expressed (denoted $\psi_D^{d(n)}$ and $\psi_A^{d(n)}$), thus giving perspective needed to interpret the differences between 2-st and multistate frameworks (superscripts a(n) and d(n) will be used to denote, respectively, adiabatic and diabatic states in an n-space). Even in cases that the 2-st model is adequate for modeling ET kinetics, a multistate

† Part of the "Michael R. Wasielewski Festschrift".

* Corresponding authors. E-mails: (R.J.C.) robert_cave@hmc.edu; (M.D.N.) newton@bnl.gov.

§ Present address: Department of Chemistry, Yale University, New Haven, CT 06520.

⊥ Present address: Department of Chemistry, Michigan State University, East Lansing, Michigan 48824.

10.1021/jp102353q
Published on Web 07/22/2010

analysis may still be valuable in facilitating the decomposition of D/A coupling in terms of superexchange (se) coupling.[13,32]

The present paper is motivated by a number of questions related to the above issues. What is the most appropriate reduced electronic space ($n \geq 2$) for modeling ET processes? When is the 2-st model adequate, bearing in mind the debate and analysis in the recent literature (Bixon et al.,[28] Gould et al.,[29] Cave and Newton,[31] Rust et al.,[25] Voityuk,[18,19] Lambert et al.,[20,21] and Nelsen et al.[22])? What is the appropriate set of states, either adiabatic (eigenstates) or diabatic states (initial, final, etc.) to be employed in modeling ET within the chosen space? More specifically, what precise operational definitions are suitable for expressing these states? In this context, what are the distinctions between various common descriptors such as "zeroth-order", "bare", "localized", "true", and "real" diabatic states and associated D/A coupling, and once suitable D and A states have been identified, how can one determine quantitatively if the strength of D and A mixing with bridge (B) states is weak enough to justify the use of a 2-st se model (e.g., in a golden rule (GR) model for the ET rate constant, k_{ET}).[2,6,8] In the remainder of the paper, we label the states according to the dominant contribution (D, A, B, etc.). Finally, how can the preceding questions be addressed in a framework amenable to computational implementation and contact with experiment? After explaining the theoretical and computational methodology, calculated results are presented for some binuclear Ru complexes, which were the subject of a previous computational study.[33]

II. Electronic States and Spaces

A. Electronic Spaces. The electronic space is taken as an adiabatic space (n-space) consisting of n eigenstates of the electronic Born−Oppenheimer (BO) Hamiltonian, H^{el}, with n as small as possible, while still encompassing the D and A manifolds pertaining to the ET process of interest (in the following, the superscript "el" will be suppressed). The relevant D and A manifold also must take adequate account of the role of any intervening bridge states (B).[13,14,16,22,32,34,35] Quantitative means of assessing the degree to which this criterion is satisfied are considered below over a range of n values for a given ET system. The spaces adopted here are based on in vacuo adiabatic states, but may also be defined as in situ spaces (e.g., in the presence of a variable solvent reaction field).[36−39] A many-electron state space can often be represented to good approximation in terms of a space of orbital eigenfunctions (e.g., self-consistent field (SCF) orbitals, as employed in the present study), with H_{DA} taken as h_{DA}, where h is an effective 1-electron (1-e) Hamiltonian, and D and A are donor and acceptor orbitals (see section IIIB).[15,37,40−43]

B. Electronic States. The chosen space for modeling ET may be represented using the adiabatic states themselves or, for convenience, a linear transformation to a diabatic basis (the two representations can be shown to give equivalent account of D/A coupling[2]). Diabatic states are not uniquely defined and should be based on a suitable physically motivated criterion (section III).

Within the selected adiabatic space, the desired diabatic states may be defined as eigenstates of some operator other than the full electronic Hamiltonian: for example, a reference Hamiltonian or some other operator. Before proceeding to our particular choice of operator, we offer a few comments about terminology for different types of diabatic states. States fully localized on various atomic or molecular sites (e.g., by truncation of off-site contributions, a procedure easily implemented when an atom-centered basis set is employed) are one candidate for zeroth-order reference or "bare" diabatic states (denoted ψ_D^0, ψ_A^0, ψ_B^0, etc.).[13,16] Direct coupling between ψ_D^0 and ψ_A^0 on different sites is generally referred to as *through-space* coupling (H_{DA}^0), although in the presence of bridge or other nearby groups, it is not clear what this quantity means due to effects arising when the states are required to be orthogonal.[13,44,45] Alternatives to such strictly localized states (ψ_i^0) will be considered below in comparing diabatic results from different n-spaces.

When the constraint of strict localization is relaxed, the "true" or "dressed" diabatic states (denoted as $\psi_i^{d(n)}$ and defined according to whatever physical criterion and n-space is adopted), while still having the transferring charge primarily localized on the various sites (D, A, B, etc.), will typically incorporate tails extending onto neighboring sites, especially in the case of bridge-mediated ET, where the D and A tails on the bridges are the essence of the superexchange (through-bond) coupling entailed in $H_{DA}^{d(n)}$ for a DBA system.[13,32] The generalized Mulliken Hush (GMH)[31,46] criterion (section III) maximizes the localization of $\psi_D^{d(n)}$ and $\psi_A^{d(n)}$ along the charge transfer direction (subject to orthogonalization); these states may be more extended in perpendicular directions, as revealed in section V. As the size (n) of the adiabatic space increases, the extent of "dressing" in $\psi_D^{d(n)}$ and $\psi_A^{d(n)}$ will be found to vary. A corresponding variation is expected for the matrix elements $H_{DA}^{d(n)}$,

$$H_{DA}^{d(n)} = \langle \psi_D^{d(n)} | H | \psi_A^{d(n)} \rangle \quad (1)$$

$H_{DA}^{d(n)}$ may be re-expressed in terms of the bare functions ψ_i^0 and an n-dependent effective Hamiltonian, $H_{eff}^{(n)}$ (e.g., based on the partitioning model or the transition operator, T).[15,17,47]

$$H_{DA}^{d(n)} = \langle \psi_D^0 | H_{eff}^{(n)} \psi_A^0 | \rangle \quad (2)$$

Each of these equivalent expressions incorporates the tails noted above, with diabatic states orthogonal either by construction (as in the present work) or by explicit orthogonalization of a nonorthogonal set (e.g., Lowdin orthogonalization).[45,48]

C. "Prepared States". In general, the initial and final diabatic states are intended to represent the "prepared states" in a particular process: for example, for the purpose of evaluating H_{DA}, the initial state for thermally activated ET might correspond to the residence in the transition state (TS) occasioned by a fluctuation in the reaction coordinate (for either a ground state or a photoinitiated process when relaxation of nuclear modes is rapid), whereas for optical ET, the initial state would be the equilibrium DBA reactant.[49] For Franck−Condon contolled ET, the final state will have the same nuclear configuration as the initial state.

III. The Generalized Mulliken Hush (GMH) Model

Several formulations have been proposed for diabatic states in ET systems. For bimolecular processes, the so-called block-diagonal (BD)[31,50] method exploits a reference level based on infinitely separated reactants or truncated states at finite separation (the BD zeroth-order space is quite distinct from the analogous ψ_i^0 reference space introduced in section II). For the general case, including intramolecular processes, one can employ the symmetry-broken (SB) SCF method, applicable when distinct charge-localized (and generally non-orthogonal) initial and final SB SCF states can be obtained.[13,15,51−54] The nonperturbative GMH model[31,46] (an extension of the Mulliken Hush

model[4]) defines the maximally localized diabatic states for a charge transfer process as the eigenstates of the component of the electric dipole operator ($\hat{\boldsymbol{\mu}}$) in the direction of the overall ET process (in the following, $\hat{\boldsymbol{\mu}}$ refers to this projected component)[31,46] If this direction is not defined by symmetry, a mean direction may be obtained from the calculated results (e.g., the dipole matrix elements). A consequence of this physical criterion is that (by construction), the projected diabatic off-diagonal dipole moment matrix elements (transition moments) are zero.

Diagonalization of $\hat{\boldsymbol{\mu}}$ gives diabatic states $\psi_{\mathrm{D}}^{\mathrm{d}(n)}$ and $\psi_{\mathrm{A}}^{\mathrm{d}(n)}$, in which the separation of the D and A centroids ($r_{\mathrm{DA}}^{\mathrm{d}(n)} = (\mu_{\mathrm{AA}}^{\mathrm{d}(n)} - \mu_{\mathrm{DD}}^{\mathrm{d}(n)})/e$) is maximized. We represent this procedure in terms of the following $n \times n$ matrices:

$$\boldsymbol{\mu}^{\mathrm{d}(n)} = (\mathbf{U}^{\mathrm{d}(n)})^{\dagger}\, \boldsymbol{\mu}^{\mathrm{a}(n)}\, \mathbf{U}^{\mathrm{d}(n)} \tag{3}$$

$$\mathbf{H}^{\mathrm{d}(n)} = (\mathbf{U}^{\mathrm{d}(n)})^{\dagger}\, \mathbf{H}^{\mathrm{a}(n)}\, \mathbf{U}^{\mathrm{d}(n)} \tag{4}$$

where $H_{\mathrm{ij}}^{\mathrm{a}(n)}$ and $\mu_{\mathrm{ij}}^{\mathrm{d}(n)}$ are diagonal by construction: $\mu_{\mathrm{ij}}^{\mathrm{d}(n)} = \mu_{\mathrm{ii}}^{\mathrm{d}(n)}\delta_{\mathrm{ij}}$ and $H_{\mathrm{ii}}^{\mathrm{a}(n)} = H_{\mathrm{ii}}^{\mathrm{a}(n)}\delta_{\mathrm{ij}}$.

The localization inherent in the GMH approximation assumes a distance scale separation in which $r_{\mathrm{DA}}^{\mathrm{d}(n)}$ is large relative to the spatial extent of the local states in the ET direction ($\sigma_{\mathrm{D}}^{\mathrm{d}(n)}$ and $\sigma_{\mathrm{A}}^{\mathrm{d}(n)}$, etc), which may be expressed as suitable second moments of the state charge densities ($\sigma = ((|\mu - \mu_{ii}|^2)_{ii})^{1/2}/\mathrm{e}$, where i denotes D or A). When a given site has more than one local state, $H_{ij}^{\mathrm{d}(n)}$ for each such block is rediagonalized, as denoted collectively by the locally adiabatic (la) transformation, $\mathbf{U}^{\mathrm{la}(n)}$, so that eqs 3 and 4 are updated as

$$\mathbf{H}^{\mathrm{la}(n)} = (\mathbf{U}^{\mathrm{la}(n)})^{\dagger}\, \mathbf{H}^{\mathrm{d}(n)}\, \mathbf{U}^{\mathrm{la}(n)} \tag{5}$$

$$\boldsymbol{\mu}^{\mathrm{la}(n)} = (\mathbf{U}^{\mathrm{la}(n)})^{\dagger}\, \boldsymbol{\mu}^{\mathrm{d}(n)}\, \mathbf{U}^{\mathrm{la}(n)} \tag{6}$$

In the following, we retain the notation $\mathbf{H}^{\mathrm{d}(n)}$ and $\boldsymbol{\mu}^{\mathrm{d}(n)}$, assuming that any necessary local adiabaticity has been imposed. In the present study, the n-spaces selected contain only a single diabatic state on the D ($\psi_{\mathrm{D}}^{\mathrm{d}(n)}$) and A ($\psi_{\mathrm{A}}^{\mathrm{d}(n)}$) sites, and these states are unaffected by la transformation involving other diabatic states (in general, the la transformation impacts coupling when D and A sites include more than a single state).

A. 2-st ($n = 2$). The GMH model for $H_{\mathrm{DA}}^{\mathrm{d}(2)}$ is compactly expressed at the 2-st level:

$$H_{\mathrm{DA}}^{\mathrm{d}(2)} = -\Delta E_{12}^{\mathrm{a}(2)}\, \mu_{12}^{\mathrm{a}(2)}/\left(\left(\Delta\mu_{12}^{\mathrm{a}(2)}\right)^2 + 4\left(\mu_{12}^{\mathrm{a}(2)}\right)^2\right)^{1/2} \tag{7}$$

relating diabatic and adiabatic energy ($\Delta E_{12}^{\mathrm{a}(2)} \equiv H_{22}^{\mathrm{a}(2)} - H_{11}^{\mathrm{a}(2)}$) and dipole quantities (where $\Delta X_{ij}' \equiv X_j - X_i$). In turn, the denominator in eq 8 is proportional to $r_{\mathrm{DA}}^{\mathrm{d}(2)}$,

$$\mathrm{er}_{\mathrm{DA}}^{\mathrm{d}(2)} = \Delta\mu_{\mathrm{DA}}^{\mathrm{d}(2)} = \left(\left(\Delta\mu_{12}^{\mathrm{a}(2)}\right)^2 + 4\left(\Delta\mu_{12}^{\mathrm{a}(2)}\right)^2\right)^{1/2} \tag{8}$$

Thus, via eqs 7 and 8, $H_{\mathrm{DA}}^{\mathrm{d}(2)}$ and $r_{\mathrm{DA}}^{\mathrm{d}(2)}$ may be determined entirely from adiabatic results, requiring no additional information, such as population analysis, and no ad hoc assumptions about D and A states: that is, the information about diabatic coupling in thermal, nonradiative ET is contained in the adiabatic quantities pertinent to the energy gap and intensity of the corresponding radiative optical process. The adiabatic information needed to evaluate $H_{\mathrm{DA}}^{\mathrm{d}(2)}$ may be obtained from either computational (e.g., many-electron configuration interaction (CI) or SCF calculations) or experimental (e.g., Stark spectra[55,56]) sources. This situation, explicitly displayed for $n = 2$ (eq 7), is general for any n-space. Combined use of computation and experiment has been pursued by Lambert et al. for 3-st GMH models, for which calculated magnitudes and signs of some dipole quantities are used to supplement optical data.[20,21] Another great advantage of GMH is that it can be applied to an arbitrary molecular configuration, thus permitting tests of the Condon approximation.[57]

In eqs 7 and 8, the diabatic (D, A) and adiabatic (1, 2) states are related by the following transformation,

$$\langle DA| = \langle 12| \begin{pmatrix} \cos\eta & -\sin\eta \\ \sin\eta & \cos\eta \end{pmatrix} \tag{9}$$

where $\tan(2\eta) = -2\mu_{12}^{\mathrm{a}(2)}/\Delta\mu_{12}^{\mathrm{a}(2)}$. The sign of $H_{\mathrm{DA}}^{\mathrm{d}(2)}$ is a physical observable, but contingent on phase conventions for $\psi_{\mathrm{D}}^{\mathrm{d}(2)}$ and $\psi_{\mathrm{A}}^{\mathrm{d}(2)}$, as discussed in section V.[13] When $H_{\mathrm{DA}}^{\mathrm{d}(2)}$ is squared, as in the GR rate constant expression, the sign is irrelevant, but in general ($n > 2$), interference effects may occur (see sections II, V, and VI). Even for $n = 2$, the overall coupling, $H_{\mathrm{DA}}^{\mathrm{d}(2)}$, implicitly contains through-space as well as through-bond (se) amplitudes whose superposition may lead to appreciable interference. The signs of $H_{\mathrm{DA}}^{\mathrm{d}(2)}$ reported below are based on the convention that the phases of $\psi_{\mathrm{D}}^{\mathrm{d}(2)}$ and $\psi_{\mathrm{A}}^{\mathrm{d}(2)}$ are chosen so that they are "in phase" with each other (i.e., in a formally "bonding" situation, such as for orbitals of type d_{xz} (D) and $-\mathrm{d}_{xz}$ (A), if sites D and A lie along a common z axis. This convention is suitable for the DBA complexes addressed below, although in other cases, the "bonding" relationship may be ambiguous.[58]

In the limit of symmetry-equivalent D and A sites, eq 7 becomes the familiar expression,

$$H_{\mathrm{DA}}^{\mathrm{d}(2)} = -\Delta E_{12}^{\mathrm{a}(2)}/2 \tag{10}$$

applicable to the TS for thermal electron exchange or the equilibrium geometry for optical excitation in a Robin/Day Class III system.[59] In the latter delocalized situation, there is no net ET ($\Delta\mu_{12}^{\mathrm{a}(2)} = 0$), but in the diabatic (partially localized) representation, $r_{\mathrm{DA}}^{\mathrm{d}(2)} \neq 0$ (eq 8), and the optical excitation may be viewed as a superposition of exactly compensating ET transitions. In the Class III case, the adiabatic states $\psi_1^{\mathrm{a}(2)}$ and $\psi_2^{\mathrm{a}(2)}$ will transform according to different irreducible representations (irreps), but the optical process will be dipole-allowed if the product of $\psi_1^{\mathrm{a}(2)}$ and $\psi_2^{\mathrm{a}(2)}$ transforms as the dipole operator in the D/A direction. On the other hand, $H_{\mathrm{DA}}^{\mathrm{d}(2)}$ (eq 7) will in general be finite, since the product of symmetry-equivalent diabatic states ($\psi_{\mathrm{D}}^{\mathrm{d}(2)}$ and $\psi_{\mathrm{A}}^{\mathrm{d}(2)}$) contains the totally symmetric irrep in the point group of the Hamiltonian.

B. Case of $n > 2$. For larger n-spaces ($n > 2$), the details of the effective D and A states ($\psi_{\mathrm{D}}^{\mathrm{d}(n)}$ and $\psi_{\mathrm{D}}^{\mathrm{d}(n)}$ are expected to change (as governed by the transformation $\mathbf{U}^{(n)}$ in eqs 3−6) and, hence, also the values of $H_{\mathrm{DA}}^{\mathrm{d}(n)}$ and $\Delta\mu_{\mathrm{DA}}^{\mathrm{d}(n)}$. The quantity $r_{\mathrm{DA}}^{\mathrm{d}(n)}$ retains its natural definition as the separation distance of the D and A centroids ($\Delta\mu_{\mathrm{DA}}^{\mathrm{d}(n)}/e$). A larger n-space may in general include states representing e and h transfer through a bridge (involving, respectively, the unoccupied and occupied orbitals of B), as well as additional states on D and A or other sites. A balanced n-space is necessary to ensure the appropriate inclusion of interference effects. Diagnostic tests of 2-st results can indicate the possibility of appreciable differences in coupling

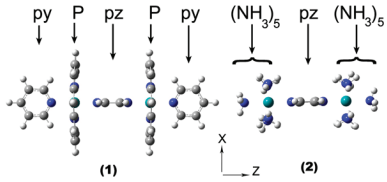

Figure 1. Optimized structures of the reduced (Ru^{2+}/Ru^{2+}) binuclear Ru complexes **1** (D_{2h}) and **2** (C_2), with net charges, respectively, of 0 and 4+ and with *y* the C_2 axis. The py, pz, P (porphinide), and NH_3 ligands are indicated above each complex. The Ru, C, N, and H atoms are indicated, respectively, by cyan, gray, blue, and white spheres. The heavy-atom framework of **2** has $\sim D_{2h}$ symmetry, and the py and pz moieties in **1** and **2** are essentially planar, with the *x*-axis perpendicular to the pz plane.The atoms of the P ligands lie nearly in the *xy* planes containing the Ru atoms. In **3** (optimized D_{2h} structure, not shown), the outer axial ligands of **1** (py) are replaced by CO ligands.

magnitude for larger n-spaces, and approximate means of adjusting 2-st results have been formulated.[25] Trends with increasing *n* and indications of "convergence" are explored in section V (see also ref 34). A proposal for defining the "optimal" *n*-space (in which the magnitude of the total excess charge at the D and A sites, as obtained by population analysis of the entire $\psi_i^{d(n)}$ manifold, approaches unity as closely as possible) has also been suggested.[34]

In cases that a mean ET direction is not well-defined for $n > 2$ (e.g., in cases of multiple D and A sites), a more general diabatization scheme has been reported.[60,61] When the rate of ET is very weak or symmetry forbidden (either optically, due to the transition moment, or thermally, due to $H_{DA}^{d(n)}$), an electronic model such as GMH should be extended to include vibronic coupling (either non-Condon (Herzberg−Teller) or non-BO state mixing).[28,62−64]

IV. Calculations

A. Molecular Systems. Properties of diabatic states in variable *n*-spaces are examined for mixed valence (MV) Ru complexes (Ru^{2+}/Ru^{3+}) involving a central ($(Ru-pz-Ru)^{5+}$ moiety (pz′ pyrazine), in which the superscripts denote nominal oxidation states. Primary attention is focused on a porphinide (P) complex with axial pyridine (py) ligands, **1** (Figure 1a), and the Creutz−Taube (C-T) complex,[65,66] **2** (Figure 1b). Comparison is also made with complex **3** (not displayed), in which the outer axial py ligands of **1** are replaced by CO ligands. Electronic structure calculations for **1**−**3** and their effective 2-st coupling elements ($H_{DA}^{d(2)}$) have been reported recently,[33] as well as experimental studies of redox and spectral behavior as a function of ligand type in related Ru complexes.[67] The sensitivity of D/A coupling in the Ru−pz−Ru moiety to variation of equatorial (P or NH_3) and outer axial (py, NH_3, or CO) ligands, along with *n*-space dependence, is analyzed in the present work.

B. Computational Models. ***1. DFT Electronic Structure and Geometry Calculations.*** The molecular structures of **1**−**3** were optimized in vacuo for the reduced binuclear complexes (Ru^{2+}/Ru^{2+}), using the B3LYP density functional[68] with the Los Alamos effective core potential and associated "double-ζ" (DZ) valence orbital basis set for Ru,[69] and all-electron treatment of other atoms, using the Dunning DZ basis.[70] The reduced molecular complexes have a net charge of either 0 (**1** and **3**, where the P ligands have nominal charges of 2−) or 4+ (**2**).

Optimized geometries for **1**−**3** possess point group symmetry, respectively, D_{2h}, C_2, and D_{2h} (the C_2 geometry of **2** has a quasi D_{2h} Ru−pz−Ru core, perturbed somewhat due to the NH_3 ligands). The equatorial Ru−N bonds of **1** and **3** are staggered relative to the nearly planar Ru−pz−Ru moiety, and the plane of the nearly planar py ligands in **1** is orthogonal to the Ru−pz−Ru plane. The coordinate axes are assigned as *z* along the Ru−Ru axis and *x*, perpendicular to the pz plane. The C_2 axis in **2** lies along *y*. The π-type valence orbitals of Ru and pz are respectively, $4d_{xz}$ and $2p_x$. The calculated Ru−N bond lengths have been discussed in detail in ref 33 and are found to be ∼0.1 Å larger than crystal structure values. The optimized r_{RuRu} distances are 7.020 (**1**), 7.146 (**2**), and 7.217 Å (**3**).[33]

Ideally, the structures optimized directly for the $(Ru-pz-Ru)^{5+}$ charge states of interest would be desirable, especially the $Ru-N_{pz}$ bond lengths. However, in the case of the C-T complex (**2**), for which crystal structure data is available,[71] the equilibrium $Ru-N_{pz}$ bond lengths for the 4+ and 5+ charge states are found to be very similar (1.99 ± 0.02 Å), and in both cases, the Ru sites are close to symmetry-equivalent. The 5+ charge state is thought to be an electronically delocalized Robin−Day Class III system[59] (or a borderline Class II/III system[72,73]), with nominal effective charges of +2.5 on each Ru site (i.e., a special (nonintegral) case of "mixed valence"). The 5+ oxidation state of the porphinide complex **1**, in which the coupling is found to be weaker than for **2**, is likely to be a Class II system, with nominal Ru charges of 2+ and 3+. The symmetric (D_{2h}) calculated structure for **1**, based on the 4+ charge state, thus serves as a model for the TS in the 5+ ET process. Even weaker coupling is found for **3**, for which the ground state redox process is calculated (and found experimentally[67]) to occur at the P sites, with a higher energy Ru^{2+}/Ru^{3+} redox process.

2. Effective Electronic Models for the (Ru−pz−Ru)$^{5+}$ Complexes. For analysis of diabatic states and properties, we employ a frozen orbital 1-e model[33,37] based on Kohn−Sham (KS) orbitals,[74] and the corresponding orbital energies (ε_i), and dipole matrix elements, calculated in vacuo. In this approach, which is similar in spirit to the use of Koopmans' Theorem[75] in the Hartree−Fock (HF) framework,[18,19,41,42,58] the states of the Ru^{2+}/Ru^{3+} complexes are treated in terms of the orbitals of their reduced (Ru^{2+}/Ru^{2+}) counterparts. Previous analysis for MV binuclear complexes and other DBA systems has shown the utility of such frozen orbital approaches for calculating $H_{DA}^{d(2)}$ values;[13,18,19,22,33,40,52] that is, the *many-electron* diabatic matrix element of *H* (H_{DA}) may to good approximation (i.e., typically within ∼10%[13]) be represented by the diabatic *orbital* matrix element (h_{DA}) of an effective 1-e Hamiltonian *h* (see section II). Furthermore, sample comparisons of coupling from the 1-e model (based on $(Ru-pz-Ru)^{4+}$ orbitals) and direct SCF calculations for the 5+ complexes show reasonable agreement.[33] Details of the relationship between state and orbital quantities are given in section V, after the selection of a 4-orbital space is described. In subsequent discussion of the GMH calculations, in which orbital dipole matrix elements are also employed (sections V and VIA), the term "state" will generally be used to refer to orbitals.

In the KS-orbital-based GMH model, we have

$$h_{ij}^{a(n)} = \varepsilon_i^{a(n)} \delta_{ij} \tag{11}$$

where the ε_i of the KS orbitals in the *n*-space have been relabeled $\varepsilon_i^{a(n)}$; $\Delta E_{12}^{a}(2)$ is replaced by $\varepsilon_2^{a(2)} - \varepsilon_1^{a(2)}$ in eq 7; and the $\psi_i^{a(n)}$and $\psi_i^{d(n)}$ now refer, respectively, to adiabatic and diabatic orbitals in an orbital *n*-space. The matrix elements of *h* in the $\psi_i^{d(n)}$ basis are denoted as $h_{ij}^{d(n)}$. For $n \geq 4$, with two states on the pz sites (π and π*), the corresponding 2×2 block of *h* (generated by the standard GMH model) is diagonalized (the la situation

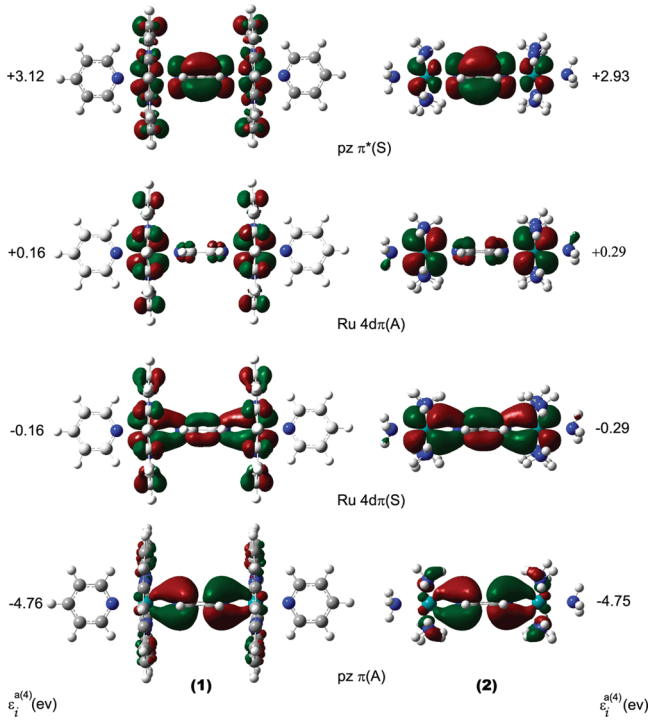

Figure 2. Four-state adiabatic spaces for **1** and **2** ($\psi_i^{a(4)}$). The Ru orbitals are of the 4dπ_{xz} type. Symbols S and A denote symmetry or antisymmetry with respect to the *xy* reflection plane of **1** (respectively, b_{3u} and b_{2g} in D_{2h}) and the quasi reflection plane of **2** (respectively, *b* and *a* in C_2). Red and green distinguish positive and negative orbital lobes, and atoms are assigned the same colored spheres as in Figure 1. The $\varepsilon_i^{a(4)}$ are the KS DFT orbital energies, shifted so that zero is the energy of the degenerate orbitals $\psi_D^{d(2)}$ and $\psi_A^{d(2)}$ (shown in Figure 3).The zero chosen here corresponds to −4.615 eV (**1**) and −16.759 eV (**2**) on the KS orbital energy scale. Labels Ru and pz denote the major contributor to each orbital.

mentioned in section III) and then $\boldsymbol{\mu}^{d(n)}$ is transformed to the la basis. Note that the *strict* 1-e model employed here is distinct from an alternative approach in which the many-electron *H* was approximated as a sum of effective 1-e Hamiltonians expressed in an assumed diabatic basis[12] (see also ref 13).

V. GMH Results

Most of the GMH analysis involves $n = 2$, 3, or 4 ($n = 5$ is also considered for **1**, and $n = 6$, for **3**). Figure 2 displays the four KS SCF orbitals (i.e., the adiabatic states in the present 1-e model, ordered from bottom to top according to increasing $\varepsilon_i^{a(4)}$) most important for coupling in the $(Ru-pz-Ru)^{5+}$ unit of **1** and **2** (the analogous orbitals for **3** (not shown) are qualitatively similar): states $\psi_2^{a(4)}$ and $\psi_3^{a(4)}$ (middle of figure), with the major Ru 4d_{xz} contributions, and $\psi_1^{a(4)}$ (bottom) and $\psi_4^{a(4)}$ (top) dominated, respectively, by the highest occupied (π) and lowest unoccupied (π^*) pz π-type molecular orbitals (MO), which have finite amplitude on the N-atoms (i.e., the atoms linked to the Ru atoms). The zero of energy is defined as the energy of the degenerate $\psi_D^{d(2)}$ and $\psi_A^{d(2)}$ shown in Figure 3 (see caption for Figure 2).

In the selection of the adiabatic 4-space described above (similar to the procedure employed in ref 22), $\psi_3^{a(2)}$ is the highest occupied MO (homo), and $\psi_2^{a(2)}$ is found to be homo-3 (**1**) and homo-5 (**2**).[33] The π and π^* pz orbitals are, respectively, homo-38 and lumo +4 (**1**) and homo-14 and lumo (**2**), where lumo denotes the lowest unoccupied MO.

With respect to the actual (for **1**) or approximate (for **2**) D_{2h} reflection plane bisecting the Ru−Ru vector, the $\psi_i^{a(4)}$ are,

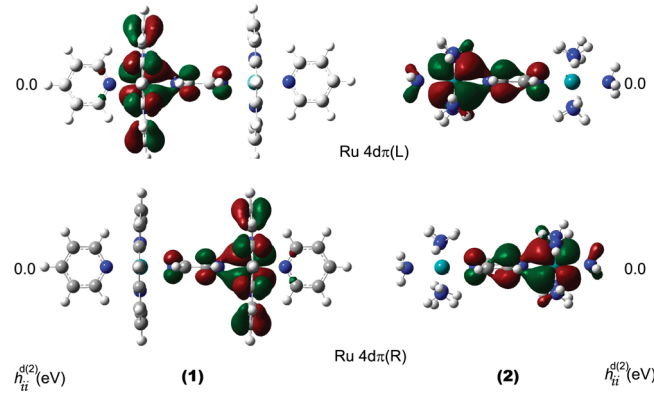

Figure 3. Two-state GMH diabatic orbitals for **1** and **2**, $\psi_D^{d(2)}$ and $\psi_A^{d(2)}$. These symmetry-equivalent orbitals are distinguished as the left-hand (L) and right-hand (R) localized states. The energy scale for the $\varepsilon_i^{d(2)}$ is given in the Figure 2 caption.

respectively of A, S, A, and S symmetry (symmetric or antisymmetric). In D_{2h} symmetry, A and S correspond, respectively, to irreps b_{2g} and b_{3u}. The orbitals are superimposed on the structures a and b of Figure 1.

In the 4-st space, the ground state (G) corresponds to the orbital occupations $(1)^2(2)^2(3)^1$.

Some orbital transitions of interest in order of increasing excitation energy are intervalence transfer (IT), 2 → 3; metal-to-ligand charge transfer (MLCT), 3 → 4; ligand-to-metal charge transfer (LMCT), 1 → 3; and also the pz $\pi \rightarrow \pi^*$ transition ($\pi\pi^*$), 1 → 4, although the high-energy $\pi\pi^*$ state is of minor importance for coupling in the Ru−pz−Ru complexes. In terms of the $\varepsilon_i^{a(4)}$, the energy gaps for the above transitions are approximated in the 1-e model as $\varepsilon_3^{a(4)}-\varepsilon_2^{a(4)}$ (IT), $\varepsilon_4^{a(4)}-\varepsilon_3^{a(4)}$ (MLCT), $\varepsilon_3^{a(4)}-\varepsilon_1^{a(4)}$ (LMCT), and $\varepsilon_4^{a(4)}-\varepsilon_1^{a(4)}$ ($\pi\pi^*$). These orbital transitions (originating from G) are the lowest energy examples of each of the four generic types of excitation. Additional excitations of the MLCT and $\pi\pi^*$ type are also possible.The transition dipole moments ($\mu_{ij}^{a(4)}$) linking the four orbitals ($\psi_i^{a(4)}$) cover the same set as those that would be obtained for the corresponding many-electron states associated with the various IT, MLCT, LMCT, and $\pi\pi^*$ transitions, although there is no simple 1−1 relationship between the orbitals and many-electron states (the latter involve spin-adapted configurations consisting of either one or three half-filled MO's) and no simple relationship between 1-e and many-electron transition dipole moments ($\mu_{ij}^{a(4)}$) for excitations in which an electron−hole pair is created.

The ability of the present strict 1-e model based on approximate (B3LYP, with a modest orbital basis) KS orbital energy gaps to provide useful estimates of the energy gaps for the $(Ru-pz-Ru)^{5+}$ system is not immediately clear. However, some comparisons with experiment for **2**, included in section VI, suggest reasonable agreement, thus supporting the use of the present model for evaluating and analyzing coupling elements in different multistate situations.

A. Comparison of Results for Different *n* Values. ***1. Adiabatic and Diabatic Orbitals.*** In complex **1**, the P ligands make notable contributions to the four adiabatic orbitals, $\psi_1^{a(4)}$, whereas those due to the axial py ligands are negligible at the resolution displayed in Figure 2 (a threshold of 0.02 au). Likewise, the ammine ligands in **2** make very minor contributions (Figure 2). The orbital with the "bonded" Ru−Ru interaction in $\psi_2^{a(4)}$ (i.e., left (L)- and right (R)-hand 4d_{xz} color-coded lobes are in-phase (S)) lies below the orbital ($\psi_3^{a(4)}$) with the out-of-phase (A) pairing in Figure 2. The Ru−pz bonding and antibonding interactions are visible in Figure 2. Note that $\psi_3^{a(4)}$, which is

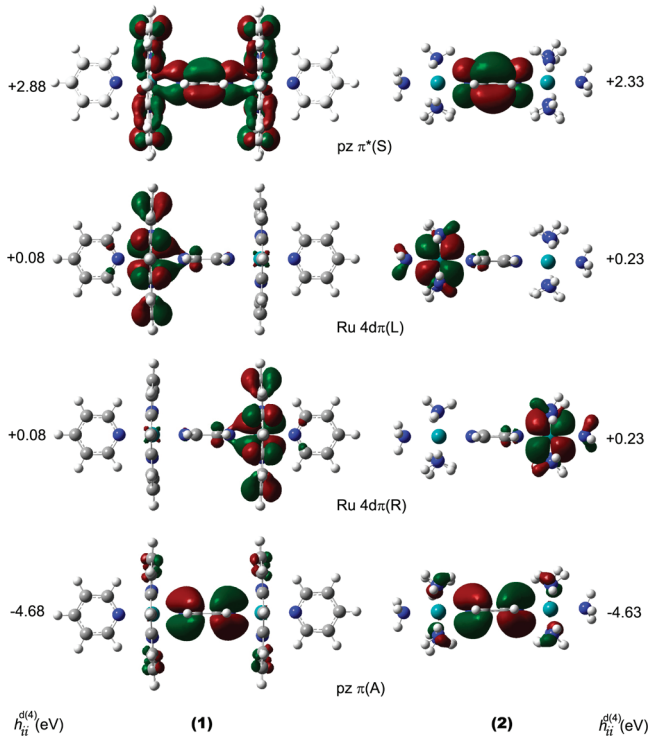

Figure 4. Four-state diabatic orbitals for **1** and **2**, $\psi_i^{d(4)}$. The pz orbital pair, belonging to a 2 × 2 locally adiabatic (la) block (see section III and eqs 5 and 6) retains S/A symmetry while being more localized on pz relative to their adiabatic counterparts in Figure 2. The energy scale for $\varepsilon_i^{d(4)}$ is given in the Figure 2 caption.

nominally labeled nonbonding in simple 3-st models,[76] exhibits a small degree of Ru−pz antibonding character.

The GMH procedure (section III) has been implemented for **1** and **2** using the set of four adiabatic states (4-st) or a subspace (2-st or 3-st). For the $n = 2$ and 3 cases, the larger 4-space can serve as a variant of the zeroth-order reference basis, ψ_i^0, introduced in section II. The results for **3** are discussed below. Diabatic states for **1** and **2** at the 2-st level ($\psi_D^{d(2)}$and $\psi_A^{d(2)}$) are displayed in Figure 3, and for comparison, the 4-st orbitals ($\psi_i^{d(4)}$) are shown in Figure 4. The 2-st results exhibit notably less Ru−pz mixing (especially for **2**) than in the corresponding adiabatic orbitals, $\psi_2^{a(4)}$ and $\psi_3^{a(4)}$ (cf., Figures 2 and 3). Nevertheless, for **1**, the Ru−pz mixing in $\psi_D^{d(2)}$ and $\psi_A^{d(2)}$ is still appreciable, displaying net bonding character, dominated by Ru dπ−pz π* backbonding (MLCT). The equatorial Ru−P mixing in **1**, while not directly affected by the GMH localization along the Ru−Ru axis see section III) is also substantial. The 4-st D and A orbitals for **1** and **2**, $\psi_D^{d(4)}$ and $\psi_A^{d(4)}$ (see Figure 4), are more localized on their respective Ru atoms than their 2-st counterparts, but for **1**, they maintain Ru−P mixing.

2. $h_{DA}^{d(n)}$ and $r_{DA}^{d(n)}$. GMH results for $h_{DA}^{d(n)}$ and $r_{DA}^{d(n)}$ are presented in Table 1 (the se quantities are discussed below). In addition to the 2-st and 4-st results, Table 1 also includes results for intermediate-sized spaces (3-st), in which either the pz occupied π ($\psi_1^{a(4)}$) or unoccupied π* ($\psi_4^{a(4)}$) adiabatic orbitals are included. The 3-st cases are denoted as $n = 3$ (π) or $n = 3^*$ (π*) and are introduced to help in elucidating the contributions of the pz π and π* orbitals to the effective D/A coupling and the nature of interference effects between the two se pathways (respectively, h and e types).

Table 1 together with Figures 2−4 indicate a monotonic increase in localization of $\psi_D^{d(4)}$ and $\psi_A^{d(4)}$ as n increases from 2 to 4. In particular, the tails of $\psi_D^{d(4)}$ and $\psi_A^{d(4)}$ extending onto the pz bridge are reduced, $h_{DA}^{d(n)}$ becomes less negative (or more positive, comparing 3* and 4 for **2**), and $r_{DA}^{d(n)}$ is increased for both **1** and **2**. The negative sign for most of the $h_{DA}^{d(n)}$ values corresponds to the coupling of D and A states in a "bonding" (in phase) relationship (i.e., mirror equivalent pair), as noted in section IV.

TABLE 1: GMH $h_{DA}^{d(n)}$ Values for Complexes 1 and 2 (10^3 cm^{-1})[a]

complex[b]	n[c]	$h_{DA}^{d(n)}$	$\Delta h_{DA}^{se-d(n)}$	$h_{DA}^{se-d(n)}$	$r_{DA}^{d(n)}/r_{RuRu}$
1	2 (D, A)	−1.36			0.92
	3 (D, A, π(pz))	–0.85	–0.53	–1.39	0.93
	3* (D, A, π*(pz))	–0.28	–1.19	–1.48	0.95
	4 (D, A, π, π*(pz))	–0.07	–1.38	–1.45	0.97
2	2 (D, A)	–2.39			0.87
	3 (D, A, π(pz))	–1.18	–1.32	–2.50	0.90
	3* (D, A, π*(pz))	+0.32	–3.61	–3.29	0.98
	4 (D, A, π, π*(pz))	+0.49	–3.52	–3.03	0.99

[a] Matrix elements of h defined in eqs 10−14. For discussion of sign conventions, see section VA1 and Figures 2−4. $r_{DA}^{d(n)} \equiv \Delta\mu_{DA}^{d(n)}/e$ (see eqs 3, 6, and 8). r_{RuRu} is the DFT-optimized Ru−Ru separation distance (see section VA1). [b] Structures of **1** and **2** are given in Figure 1. [c] Size and composition of the n-space; D, A, π, and π* correspond, respectively, to $\psi_D^{d(n)}$, $\psi_A^{d(n)}$, $\psi_{\pi(pz)}^{d(n)}$, and $\psi_{\pi^*(pz)}^{d(n)}$ (obtained from the $\psi_i^{a(n)}$ at the n-st GMH level). The se quantities are based on eqs 12−15.

As an additional test of n-dependence, 5-st calculations were carried out for **1**, adding the KS lumo (mostly involving the P orbitals, with very little Ru 4dπ contribution) to the 4-space. The results, $\psi_D^{d(5)}$ and $\psi_A^{d(5)}$, are more localized than their 4-st counterparts ($r_{DA}^{d(n)}/r_{RuRu} = 0.99$), and the coupling $h_{DA}^{d(5)} = +0.36$ x 103 cm^{-1}, larger in magnitude than for $n = 3^*$ and 4, but with opposite sign, thus reinforcing the monotonic trends displayed in Table 1.

To assess these results further, we let a larger n-space ($n =$ 3 or 4) serve as a zeroth-order reference space for the 2-st wave functions, $\psi_D^{d(2)}$ and $\psi_A^{d(2)}$; that is, the ψ_i^0 introduced in section II are taken as $\psi_i^{d(n)}$, with $n = 3$ or 4. Of course, the $\psi_D^{d(n)}$ are not fully localized on D, A, or B sites, etc., but they are still useful as a reasonably localized reference basis for analyzing the 2-st model. The matrix elements $h_{DA}^{d(n)}$, $n = 3$ or 4, provide estimates of "bare" or direct (through space) coupling. Residual coupling due to the larger space represented by the full manifold of KS SCF orbitals is implicitly contained in the coupling dicussed here explicitly for $n \leq 4$. Calculations with the pz ligands removed yield direct coupling magnitudes of <10 cm^{-1}.

3. Superexchange (se) Models. We first employ a se model[13,14,32,35] to construct a PT estimate of $\psi_D^{d(2)}$ and $\psi_A^{d(2)}$ coupling for comparison with the actual 2-st ($h_{DA}^{d(2)}$) result:

$$h_{DA}^{se-d(n)} = h_{DA}^{d(n)} + \Delta h_{DA}^{se-d(n)} \tag{12}$$

$$\Delta h_{DA}^{se-d(n)} = \sum_{i,j=3}^{n} h_{Di}^{d(n)} \left(h_{D/A}^{d(n)} 1 - \mathbf{h}^{d(n)}\right)_{ij}^{-1} h_{jA}^{d(n)} \tag{13}$$

where

$$h_{D/A}^{d(n)} \equiv h_{DD}^{d(n)} = h_{AA}^{d(n)} \qquad \text{and} \qquad n > 2 \tag{14}$$

for the present case of symmetry-equivalent D and A sites, and i and j run over the n-space diabatic states other than $\psi_D^{d(n)}$ and $\psi_A^{d(n)}$. When orbitals i, j belong to a la block, the inverse matrix in eq 13 is diagonal, yielding the simpler se expression,

$$\Delta h_{DA}^{se-d(n)} = \sum_{i=3}^{n} h_{Di}^{d(n)} h_{iA}^{d(n)} / \Delta h_{D/Ai}^{d(n)} \quad (15)$$

where $\Delta h_{D/Ai}^{d(n)} \equiv h_{D/A}^{d(n)} - h_{ii}^{d(n)}$. Equations 13 and 15 are second-order perturbation theory results (2° PT) based on 1° PT wave functions.

The net couplings, augmented (or "dressed") by the se terms, are seen (Table 1) to be fairly close to the $n = 2$ values, as discussed in section VIA. It may also be noted that the π and π^* contributions (respectively, h and e tunneling pathways), as reflected in the 3 and 3* results in Table 1, interfere constructively (i.e., the $\Delta h_{DA}^{se-d(n)}$ terms have the same sign) in the overall tunneling represented by the 2-st results. This is also true for the π(pz) and π *(pz) contributions to $\Delta h_{DA}^{se-d(4)}$ (note that this latter quantity differs from the sum of $\Delta h_{DA}^{se-d(3)}$ and $\Delta h_{DA}^{se-d(3^*)}$ due to differences in the relevant $\psi_i^{d(n)}$ for $n = 3$, 3*, and 4).

4. Projection Analysis of $\psi_D^{d(n)}$ and $\psi_A^{d(n)}$. An alternative, nonperturbative, means of comparing $\psi_D^{d(n)}$ and $\psi_A^{d(n)}$ for different n values is to project the $n = 2$, 3, and 3* states onto the "bare" 4-st reference basis ($\psi_i^{d(n)}$), using the **U** matrix introduced in eqs 3−6:

$$\psi_i^{d(n)} = \sum_{j=1}^{4} P_{ij}^{(n,4)} \psi_j^{d(4)} \qquad n < 4 \quad (16)$$

$$P_{ij}^{(n,4)} = \sum_{k=1}^{n} (U^{(n)})_{ik}^{\dagger} U_{kj}^{(4)} \quad (17)$$

where i = D, A and k runs over the orbital sets defined in Table 2 for the $n = 2$, 3, and 3* spaces. Results are presented in Table 2, where each row corresponds to P_{Dj}, $j = 1-4$ (based on the assignment of the π(pz) and π^*(pz) orbitals to a 2 × 2 la block (see section III and eqs 5 and 6).

Complementing Figures 3 and 4 and Table 1, Table 2 shows quantitatively how the D and A tails penetrate the pz bridge increasingly in the sequence $n = 3^*$ to 3 to 2, dominated by backbonding to the π^*(pz) orbital for both **1** and **2**, as seen in particular by comparing results for the intermediate 3 and 3* spaces. Alternatively, extending the size of the n-space is seen to attenuate or remove the delocalized D and A tails. Even though the tails constitute at most a 10% effect, the $h_{DA}^{d(n)}$ values in Table 1 demonstrate their great importance in establishing the coupling strength. The trends in coupling can also be understood in terms of the trade-off between the implicit and explicit bridge contributions to the coupling. For example, $h_{DA}^{d(3^*)}$ in the 3* space (relative to the 2-space), retains the implicit coupling due to $\psi_{\pi(pz)}^{d(4)}$ but has the stronger coupling due to $\psi_{\pi^*(pz)}^{d(4)}$ explicitly removed (recoverable by se, to the extent that PT is valid, as shown in Table 1). In constrast, $h_{DA}^{d(3)}$ retains the implicit $\psi_{\pi^*(pz)}^{d(4)}$ coupling and, hence, is notably larger than $h_{DA}^{d(3^*)}$.

TABLE 3: GMH $h_{DA}^{d(n)}$ Values for Complex 3 (10^3 cm^{-1})[a]

n[b]	$h_{DA}^{d(n)}$	$\Delta h_{DA}^{se-d(n)}$	$h_{DA}^{se-d(n)}$	$r_{DA}^{d(n)}/r_{RuRu}$
2 (D, A)	−0.34		−0.34	1.03
4 (D, A, π, π^*(pz))	+0.23	−0.59	−0.36	1.05
6 (D, A, π, π^*(pz),π^*(CO))	+0.10	−0.56	−0.47	0.99

[a] See footnote a in Table 1 and Figure 5. [b] See footnote c in Table 1.

B. Sensitivity to Geometry. As noted in section IV, the GMH results are based on in vacuo DFT optimized geometries (with the Lan2DZ basis). These calculations tend to yield Ru−N_{pz} bond lengths ∼0.1 Å larger than crystal structure values.[33,77,78] As a test of sensitivity of $h_{DA}^{d(n)}$ to $r_{RuN(pz)}$, we have carried out GMH calculations for **2** in which the geometry is modified by replacing the optimized bond length (2.12 Å) with 2.00 Å (the crystal structure value for the 4+ and 5+ complexes). The Ru−Ru distance decreases from 7.15 to 6.91 Å. As expected, the Ru−pz mixing increases, yielding $h_{DA}^{d(2)}$ values of −3400 ($n = 2$) and +570 cm^{-1} ($n = 4$), and $r_{DA}^{d(2)}/r_{RuRu} = 84\%$ ($n = 2$) and 99% ($n = 4$), with backbonding (Ru $4d\pi_{xz}$ to pz π^*) remaining the dominant Ru−pz interaction. The $h_{DA}^{d(2)}$ values obtained in the present work with both optimized and adjusted geometries lie within the upper and lower bounds for $H_{DA}^{d(2)}$ suggested by Reimers and Hush (∼ 2400−3600 cm^{-1}).[78] The geometry (especially $r_{RuN(pz)}$) is, in turn, found to be sensitive to the basis set employed[77] and is also likely to depend on the environment of the complex (e.g., in vacuo, aqueous solution, or crystalline solid).[78] Strictly speaking, $H_{DA}^{d(2)}$ should be less than one-half the vertical gap, $\Delta E_{12}^{a(2)}$ (eq 10) by a term depending on the reorganization energy due to symmetric normal modes of the solute, a correction likely to be a few hundred cm^{-1}.[78−80]

C. Sensitivity to Axial Ligands. In complexes **1** and **2**, a pronounced feature is backbonding from Ru to the pz π-acid, the internal axial ligand, with the external axial ligands (py and NH_3) playing a passive role in the DA coupling. In striking contrast, replacing py ligands in **1** with strong π-acid CO ligands in complex **3** is known to lower the Ru πd_{xz} orbitals so that the lowest energy redox process for **3** involves the P ligand sites, with the Ru^{2+}/Ru^{3+} process occurring at higher energy. Using the KS ε values to estimate the ionization potentials (IP) of **1** and **3** (taking the mean value of ε for the S and A Ru $4d\pi$ type MOs), it is found that IP (Ru $4d\pi$) − IP (P π) = +0.2 eV (5.8 − 5.6 eV) for **3**, in contrast to −0.2 eV (4.6 − 4.8 eV) for **1**. These results are consistent with the experimental results for the mononuclear Ru complexes.[67] Even with the resonance stabilization of the $(Ru-pz-Ru)^{5+}$ moiety in complex **3** in its optimized symmetric structure ($h_{DA}^{d(2)} = -340$ cm^{-1}; Table 3), the P ligands remain the lowest energy redox sites.

TABLE 2: Delocalization Tails for 1 and 2: $\psi_D^{d(n)}$ ($n = 2$, 3, 3*) Projected[a] onto $\psi_j^{d(4)}$

complex	n[b,c]	$\psi_D^{d(4)}$	$\psi_{\pi^*(pz)}^{d(4)}$	$\psi_{\pi(pz)}^{d(4)}$	$\psi_A^{d(4)}$
1	2 (D, A)	+0.977 (95.5)	+0.192 (3.67)	−0.089 (0.79)	−0.014 (0.02)
	3 (D, A, π(pz))	+0.981 (96.2)	+0.192 (3.67)	+0.023 (0.05)	−0.018 (0.03)
	3* (D, A, π^*(pz))	+0.996 (99.2)	−0.011 (0.01)	−0.089 (0.79)	+0.005 (0.00)
2	2 (D, A)	+0.945 (89.4)	+0.304 (9.27)	−0.109 (1.18)	−0.043 (0.22)
	3 (D, A, π(pz))	+0.949 (90.1)	+0.304 (9.27)	+0.065 (0.42)	−0.047 (0.22)
	3* (D, A, π^*(pz))	+0.994 (98.8)	−0.021 (0.05)	−0.109 (1.18)	+0.006 (0.00)

[a] See section VA3 and eqs 16 and 17; signs of the projection coefficients (P_{Dj}) are based on the phases of the $\psi_j^{d(4)}$ displayed in Figure 4; squared values of P_{Dj} are displayed as percentages in parentheses. [b] $\psi_{\pi(pz)}^{d(4)}$ and $\psi_{\pi^*(pz)}^{d(4)}$ belong to a 2 × 2 la block (see section III and eqs 5 and 6). [c] See footnote c of Table 1.

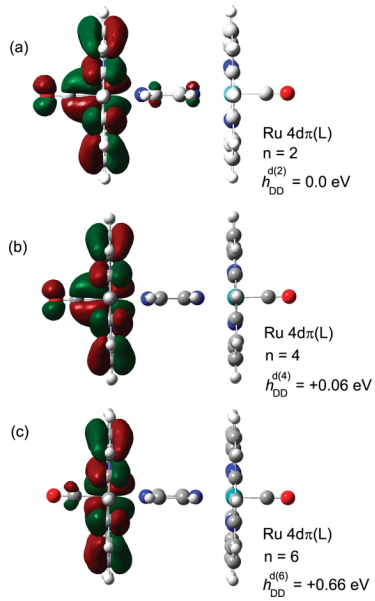

Figure 5. Diabatic donor orbitals for **3**, $\psi_D^{d(n)}$ (Ru 4dπ(L)), based on $n = 2$ (a), 4 (b), and 6 (c). The atomic spheres represent the optimized structure in the neutral charge state, with the same colors as in figures 1−4, and with red designating the O atoms. The energy scale for $\varepsilon_D^{d(n)}$ is given in the Figure 2 caption, where for **3**, the zero of energy corresponds to −5.782 eV on the scale of KS energies.

To examine the excited state Ru 4d π D/A coupling in **3**, we employ the same type of 2-st and 4-st spaces as for **1** (i.e., the Ru 4d π and pz π and π * orbitals), but in view of the expected influence of the CO π* orbitals on the coupling, we also consider a 6-st model, in which the KS CO π* type orbitals are added to the 4-space.

Results for the $n = 2$, 4, and 6-st GMH model are displayed in Figure 5 ($\psi_D^{d(n)}$), Table 3 ($h_{DA}^{d(n)}$ and $r_{DA}^{d(n)}$), and Table 4 (projection of $\psi_D^{d(2)}$ and $\psi_D^{d(4)}$ on $\psi_i^{d(6)}$, where in eqs 16 and 17 the integer variables, i = D, A; $n = 2$ and 4; and $n' = 4$ should be replaced by $n' = 6$). Note the trend of increasing localization as n increases, in conformity with the results for **1** and **2** (Table 1), and the positive values of the coupling element for $n = 4$ and 6. For $n = 2$ (Figure 5), all three ligand types contribute significantly to $\psi_D^{d(n)}$, but for $n = 4$, the pz π and π* contribution is greatly reduced. Only at the 6-st level are the CO π* orbitals essentially uncoupled from the Ru 4dπ orbitals. The competition for axial backbonding is dominated by the CO ligands, as seen in the fact that $r_{DA}^{d(n)} > r_{RuRu}$ for $n = 2$ and 4 and in the mixing coefficients shown in Table 4. The 2° PT se correction for $n = 6$ in Table 3 includes four pathways (see eq 12): two involving pz and two (more circuitous) involving the CO ligands.

VI. Discussion

A. Overview of Diabatic States and Effective Coupling. ***1. Conclusions from Present GMH Calculations.*** The GMH model provides a compact, self-contained prescription for quantitative characterization of ET diabatic states and properties, requiring no additional information, such as population analysis or effective D/A separation ($r_{DA}^{d(n)}$ follows directly from the GMH ansatz, according to which diabatic states are those that yield maximally charge-localized states along the ET direction). A primary focus has been to assess the validity of the 2-st approximation (TSA), which permits the use of the superexchange model for D/A coupling and may also permit use of the simple nonadiabatic GR expression for ET kinetics (where k_{ET} is proportional to $(H_{DA}^{d(2)})^2$), and its generalization to accommodate stronger coupling (e.g., via the Landau−Zener model)[81,82] and solvent dynamics as the adiabatic ET limit is approached. The electronic coupling plays an important role in all of these dynamical regimes. The TSA has been addressed in the context of h_{DA} values obtained from larger spaces ($h_{DA}^{d(n)}$, $n > 2$) and their dependence on space size for three different MV Ru−pz−Ru complexes (**1**−**3**).

To assess the validity of the TSA, a central issue is to specify which two states, "ψ_D" and "ψ_A", are most suitable for determining the effective coupling, h_{DA}. As emphasized above, the desired D and A states must incorporate suitable delocalized tails, as observed for the 2-st wave functions, $\psi_D^{d(2)}$ and $\psi_A^{d(2)}$, in contrast to the larger n-spaces, in which $\psi_D^{d(n)}$ and $\psi_A^{d(n)}$ become increasingly "bare". On the basis of these considerations alone, the 2-st orbitals $\psi_D^{d(2)}$ and $\psi_A^{d(2)}$ would be the preferred candidates for the effective ψ_D and ψ_A. A 2-st se model based on "bare" (zeroth-order) D and A states, however, is required to satisfy another important constraint—namely, the mixing with the bridge states or those from other sites, while crucial for establishing the effective coupling—and must conform to the demands of PT, denoted as the "weak coupling" regime by Evenson and Karplus.[16]

Focusing first on the Ru−pz−Ru moiety, we find the largest mixing is due to backbonding to the π*(pz) orbital, increasing in the order,

$$\mathbf{3} < \mathbf{1} < \mathbf{2} \tag{18}$$

with nonperturbative projection coefficients ranging from 0.12 (**3**) to 0.19 (**1**) to 0.30 (**2**). A similar trend is observed (Tables 2 and 4, and eqs 12−16) for the ratios $h_{D\pi^*}^{d(4)}/\Delta h_{D/A\pi^*}^{d(4)}$ (not shown), a measure of the vaidity of PT, ranging from ∼0.2 (**1** and **3**) to ∼0.4 (**2**). These ratios are somewhat larger than the normalized projection coefficients. The dominance of the Ru− π*(pz) mixing (backbonding) relative to the Ru−π(pz) mixing is due mainly to the respective energy denominators, $\Delta h_{D/A\pi^*}^{d(4)}$ (see Figures 4 and 5). The trend in eq 18 is also the same as that for both $h_{DA}^{d(2)}$ and $h_{DA}^{se\text{-}d(2)}$) and also the inverse trend for $r_{DA}^{d(n)}$ (Tables 1 and 3).

The extent of mixing noted above suggests that the use of PT and the se model would be valid for **1** and **3**, but less certain for **2**. For **3**, however, the situation is more complex than for **1** (cf. the coefficients for π*(CO) and π*(pz) in the first row of Table 4). The detailed 6-st calculations indicate that the se pathways involving π*(CO) contribute destructive interference to the net coupling. The rather large mixing coefficient (0.34) offers a caveat regarding the use of se for **3**.

To within a modest percentage (≤15%, based on rms deviations, and ≤38%, based on maximum deviation of $h_{DA}^{se\text{-}d(n)}$ from $h_{DA}^{d(2)}$) an "invariant" h_{DA} value is obtained (independent of n) for each complex by augmenting the "bare" (i.e., residual, implicit) coupling, $h_{DA}^{d(n)}$, for a given n, by se mixing with the states explicitly included in the n-space. This quasi invariance constitutes an internal consistency in the various n-st GMH results for coupling and provides a measure of the validity of the se model. The se terms lead to sign changes in several cases (Tables 1 and 3) as a result of destructive interference among pathways. The deviations among $h_{DA}^{d(2)}$ and $h_{DA}^{se\text{-}d(n)}$ for the three complexes (see Tables 1 and 3) are to be compared with the much larger variation of $h_{DA}^{d(n)}$ over the range of n for each complex (e.g., by as much as a factor of 20 for **1**).

In short, the se TSA in vacuo is valid for characterizing the Ru−Ru coupling in complex **1** but is perhaps of marginal validity in the case of **2** (due to stronger Ru−pz backbonding)

TABLE 4: Projection[a,b] of $\psi_D^{d(2)}$ and $\psi_D^{d(4)}$ onto $\psi_j^{d(6)}$

n[c]	$\psi_D^{d(6)}$	$\psi_{\pi^*(CO(D))}^{d(6)}$	$\psi\pi^*$(pz) d(6)	$\psi_{\pi(pz)}^{d(6)}$	$\psi_{\pi^*(CO(A))}^{d(6)}$	$\psi_A^{d(6)}$
2 (D, A)	+0.938	+0.321	+0.123	−0.043	−0.010	−0.004
	(88.0)	(10.3)	(1.52)	(0.18)	(0.01)	(0.00)
4 (D, A, π, π^*(pz))	+0.940	+0.339	−0.018	−0.006	+0.009	−0.003
	(88.4)	(11.5)	(0.03)	(0.00)	(0.01)	(0.00)

[a] The phases of $\psi_D^{d(6)}$, $\psi_A^{d(6)}$, $\psi_{\pi(pz)}^{d(6)}$, and $\psi_{\pi^*(pz)}^{d(6)}$ are the same as for the corresponding 4-st orbitals for **1** and **2** (see footnote a in Table 2); the localized CO π^*orbitals (denoted $\pi^*_{CO(D)}$ and $\pi^*_{CO(A)}$) are in phase (i.e., "bonding") with the Ru $4d\pi_{xz}$ orbitals (D and A), as depicted in Figure 5. [b] $\psi_{\pi(pz)}^{d(6)}$ and $\psi_{\pi^*(pz)}^{d(6)}$ belong to a 2 × 2 la block (see section III and eqs 5 and 6). [c] See footnote c in Table 1.

and **3** (due to the strong backbonding to the external axial CO ligands). In condensed phases, the validity of the se TSA would be influenced by the effect of the environment on the local sites.[78] With regard to dynamics or kinetics, the coupling in all three complexes is strong enough to be at or near the adiabatic limit, thus precluding the use of the GR in modeling rate constants. In any case, the two states appropriate for the effective D/A coupling when the TSA *is* valid are $\psi_D^{d(2)}$ and $\psi_A^{d(2)}$, and not the more localized (bare) D and A states, which we have obtained for $n > 2$ ($\psi_D^{d(n)}$ and $\psi_A^{d(n)}$).

The trend of increasing localization with n and the attenuation of the tails extending onto the pz bridge is evident not only in the magnitudes of $h_{DA}^{d(n)}$ and $r_{DA}^{d(n)}$ (Tables 1 and 3) and the projection coefficients, P_{Dj} (Tables 2 and 4), but also in the change of signs exhibited by $h_{DA}^{d(n)}$ in several cases for the largest n-spaces sampled. It is likely that the change of sign as n is increased is indicative of residual destructive interference with pathways involving other higher-lying localized states. However, the magnitude of $h_{DA}^{d(n)}$ remains considerably smaller than $h_{DA}^{d(2)}$, indicating that this interference is relatively small.

Concerning the issue of "convergence" of diabatic state properties with respect to n for **1**−**3**, the generally monotonic decrease of $h_{DA}^{d(n)}$ with n (and increase of $r_{DA}^{d(n)}$) found here is an interesting preliminary finding, but any general conclusion would require considerably more computational information based on a larger range of n.

2. Contact with Experiment. Aside from extended computational efforts, clearly, a comparison with coupling elements inferred from experiment will be essential in validating and arbitrating among different models and operational definitions of effective D and A states and their coupling. Comparison with experiment has not been the focus of this study, but we emphasize that despite the approximate nature of the frozen orbital model used here, the calculated energy gaps seem in reasonable agreement with experiment in the few cases for which comparison can be made: for example, for **2**, the in vacuo calculated adiabatic gaps (see Figure 2) for IT and MLCT, respectively, 0.6 and 2.6 eV, are to be compared with observed values, 0.8 and 2.2 eV.[65,66,83] The IT band is thought to be sensitive to medium (including the influence of medium on intramolecular structure),[78] and dielectric continuum-based (DC) reaction field (RF) models may be of some use in modeling the effect (e.g., see ref 37), but specific solvent effects may well be more important, as indicated, for example, by the fact that MLCT transition energies for Ru^{2+} complexes correlate monotonically with donor number, but not well with dielectric constant.[83] Related conclusions were reached by Pearl and Zerner,[84] who examined MLCT transition energies for Ru complexes using a molecular-level solvent model (QM/MM) and a DC model.

The calculated relative energetics of oxidation at Ru and P sites in **1** and **3** is consistent with experimental findings,[67] indicating a gap of ∼0.4 eV separating the oxidation energies of P and Ru in **3**.

3. GMH Results for Other ET Processes. Several GMH studies have been carried out for ET in DA or DBA systems involving a LE as well as G and CT states, using single excitation configuration interaction (CIS) wave functions at the ab initio (all-electron) or INDO/S (all-valence-electron) levels, comparing 2-st and 3-st results,[24,25,36] and in one case examining the solvent dependence of $H_{DA}^{d(n)}$ (based on a DC reaction field (RF) model).[37] The ET processes included photoinduced and optical ET for singlet state species, both neutral CS and CR ($D^*BA \rightarrow D^+BA^- \rightarrow DBA$ and $DBA \rightarrow D^+BA^-$) and cation CSh ($(D(A^+)^* \rightarrow D^+A$ and $D^+A \rightarrow DA^+$). In all cases, $H_{DA}^{d(3)}$ was found to be smaller in magnitude than $H_{DA}^{d(2)}$ (by amounts ranging from 10 to 38%), in qualitative agreement with the trend found for **1**−**3** (weaker coupling and greater localization on D and A sites).

Lambert et al. have obtained 2-st and 3-st GMH results for CSh in two series of radical cation DBA systems, with triphenylamine D and A groups and conjugated[20] or cyclophane[21] bridges (B), using AM1 CIS wave functions (and including a solvent RF for comparison with in vacuo results). For these systems, $H_{DA}^{d(3)}$ ranges from 50% smaller to 90% larger than $H_{DA}^{d(2)}$. The latter situation, which represents ∼75% of the cases, suggests the presence of special interference effects not present in the other results mentioned above. That is, for orbital spaces more complex than those depicted in Figure 2 or with different ordering of the various D, A, and spacer orbitals, cancellation of destructive interference implicit in the 2-st coupling might be reduced in the coupling elements for larger spaces, $h_{DA}^{d(n)}$, where such implicit interference is at least partially removed.

The work of Lambert et al. also reports comparison with experimental optical data and explores the promising avenue of using calculated quantities to supplement the experimental data (especially dipole matrix elements and their signs) and thus permit a complete implementation of the 3-st GMH method.

Voityuk has applied the GMH method to calculate $H_{DA}^{d(n)}$ for thermal CSh in DNA radical cations composed of duplex DNA fragments, with D and A ≡ guanine (G) and with one to three intervening adenine (A) or thymine (T) bases in each DNA strand.[18,19,34] Using ab initio HF orbitals at the KT level, he has evaluated $h_{DA}^{d(n)}$ for over 40 different DNA systems, with n ranging from 2 to as much as 8. About 50% of his results yield $h_{DA}^{d(3)}$ smaller than $h_{DA}^{d(2)}$ (by as much as 90%), and the rest, larger (by up to an order of magnitude). In these comparisons, n is generally equated to $m + 2$, where m is the number of intervening base pairs in a single strand. Once again, the wide variations with n suggest the likelihood of special interference effects (whose analysis would require the sign as well as magnitudes of all the constituent matrix elements of h). While advocating the use of $n > 2$ in GMH models, Voityuk suggests that n should not be so large as to include multiple states on a given site, thereby leading to unphysical mixing in the diabatization process. The present approach largely obviates this

possibility by imposing the locally adiabatic (la) constraint at each site (see section III).

Voityuk approximated his *n*-st GMH results using a PT model in which the zeroth-order diabatic states are taken as the 2-st results.[19] The form of this model is superficially similar to the se model introduced in section VA2 (see also ref 13), but with the important distinction that eqs 12−15 are based on the "bare" states, which we argue are the appropriate zeroth-order diabatic states, in constrast to $\psi_D^{d(2)}$ and $\psi_A^{d(2)}$, which have appreciable delocalization tails through mixing with the bridge (pz, for **1**−**3**; see Figures 3−5).

Although we have emphasized the significant differences found in some cases between 2-st and larger-state $h_{DA}^{d(n)}$ values, this fact by itself does not directly indicate which space is "better" or "more reliable", and no categorical resolution of this question seems possible at present. In the work reported here, we offer an example (**1**) in which the se model is valid and the 2-st framework provides the most appropriate expression for the effective D/A coupling element ($h_{DA}^{d(2)}$). We also show that even in the case of **2** and **3**, the se model is of semiquantitative value, even though it is quantitatively inadequate.

4. A Related Method. Nelsen et al.[22] have questioned the validity of the 2-st model for characterizing ET in a number of systems (both radical anions and cations, in the Class III or borderline regimes). In fact, part of the issue seems to be semantic. Actually, the 2-st and 4-st GMH treatment given here for the radical cations **1**−**3** is isomorphic and quite consistent with (but more complete than) the 2-st and 4-st analysis reported in ref 22 for the cation of 1,4-*N*,*N*-dimethylaminobenzene The proper 2-st results for h_{DA} are *not* the 4-st D/A pair, which we adopt as the "bare" D and A states, but rather, the $\psi_D^{d(2)}$ and $\psi_A^{d(2)}$ pair, which have been demonstrated to have delocalized tails (expressed in terms of the 4-st decomposition in Tables 2 and 4) and, thus, yield the "dressed" result, $h_{DA}^{d(2)}$ (given by eq 18 in ref 22 where the right-hand side should be multiplied by 1/2).

In the 4-st method reported ref 22, the three adiabatic gaps do not fully specify the four diabatic parameters (two energy gaps and two coupling elements, as required, for example, in the summation of eq 12, with $n = 4$), and it was concluded that a value of approximately unity was a reasonable estimate for the following ratio, R (expressed in the present notation):

$$R \equiv \left| h_{D\pi^*}^{d(4)} \Delta h_{D/A\pi^*}^{d(4)} / h_{D\pi}^{d(4)} \Delta h_{D/A\pi}^{d(4)} \right| \qquad (19)$$

where D and A are symmtry-equivalent. The 4-st GMH yields values of all four diabatic quantities on the rhs of eq 19: for **1** and **2**, we find $R \sim 0.7-0.8$, somewhat smaller than unity, but $R \sim 1.9$ for **3** (in ref 22, the bare diabatic D and A states have been symmetrically delocalized, but the resulting factors of $1/\sqrt{2}$ in the DB and BA martrix elements cancel in eq 19).

5. Intensity Borrowing. Three-state models have been employed to highlight the important role of intensity borrowing in radiative CR of the $D^+BA^- \rightarrow DBA$ type and CS of the DA* → DA type. Two such studies[28,29] have shown, starting from a model *diabatic* 3-st basis, that the omission of the LE diabatic state can lead to large underestimation of the *adiabatic* CR transition dipole. Furthermore, in the case of naphthyl D* groups, one or both steps in the photoinitiated ET sequence, $DBA \rightarrow D^*BA \rightarrow D^+BA^-$, may be spatially forbidden (or nearly so due to interference in the excited state wave function). These examples draw attention to the need in some cases for purely electronic CT models to be extended to include suitable vibronic mixing, and preliminary models have been explored.[63,64] Furthermore, in several of the cases cited,[28,29] the G → LE transition moment is likely to be perpendicular to the direction of the CS and CR dipole moment shifts, thus rendering the 3-st GMH model inapplicable, although pairwise use of the 2-st model may yield useful estimates of the G/CT and LE/CT coupling elements.

VII. Summary

Diabatic states for donor (D) and acceptor (A) interactions in electron transfer (ET) processes have been formulated and evaluated, along with coupling elements (H_{DA}) and effective D/A separation distances (r_{DA}), for reduced electronic spaces of variable size, using the generalized Mulliken Hush model, applicable to an arbitrary state space and nuclear configuration, and encompassing Robin−Day class III and as well as class II situations. With the electronic state space selected (a set of $n \geq 2$ adiabatic states approximated by an orbital space based on an effective 1-electron (1-e) Hamiltonian), the charge-localized GMH diabatic states have been obtained as the eigenstates of the dipole moment operator, with rotations to yield locally adiabatic states for sites with multiple states. The 1-e states and energies are expressed in terms of Kohn−Sham (KS) orbitals and orbital energies. Addressing questions as to whether the estimate of H_{DA} "improves" as one increases n and in what sense the GMH approach "converges" with n, we have carried out calculations for three mixed-valence binuclear Ru complexes (each with a pyrazine bridge (Ru−pz−Ru)), from which we conclude that the 2-state (2-st) model gives the most appropriate estimate of the *effective* coupling, similar (to within a rms deviation of ≤15%) to coupling elements obtained by superexchange (se) correction of H_{DA} values based on larger spaces ($n = 3-6$), and thus yielding a quasi-invariant value for H_{DA} over the range explored in the calculations ($n = 2-6$).

An analysis of the coupling and associated D and A states has shown that the 2-st coupling involves crucial mixing with intervening bridge states (D and A "tails") while increasingly larger state space for the same system yield increasingly more localized D and A states (and weaker coupling), with H_{DA} tending to approach the limit of "bare" or "through space" coupling.The mixing is dominated by Ru backbonding and for complex **3** reflects the competition between inner (pz) and outer (CO) axial π acid lgands. In terms of PT, the se model is found to be quantitatively valid for complex **1** and still useful semiquantitatively for complexes **2** and **3**. Nevertheless, for all three complexes, the overall 2-st coupling ($h_{DA}^{d(2)}$) is too strong to satisfy the separate PT requirements for use of the GR in modeling the kinetics as a nonadiabatic process. Even in other cases, when the 2-st model is adequate for modeling ET kinetics, a multistate analysis may still be valuable in facilitating the decomposition of D/A coupling in terms of the superexchange (se) model.

The present results help to reconcile seemingly contradictory assertions in the recent literature regarding the proper role of multistate frameworks in the formulation of coupling for both intra- and intermolecular ET systems.The new results presented here are compared in detail with other reported results, many of which are in conformity with the trends observed here, but with others showing different behavior. This latter behavior may reflect special interference effects arising from the qualitative features of the adiabatic states constituting the *n*-space and their relative ordering, a topic warranting further calculations and analysis.

Acknowledgment. R.J.C. gratefully acknowledges financial support from the National Science Foundation (CHE-9731634, CHE-0353199), the Donors of the Petroleum Research Fund, and Harvey Mudd College. The Division of Chemical Sciences, Geosciences, and Biosciences, Office of Basic Energy Sciences of the US Department of Energy is gratefully acknowledged for funding the research carried out by M.D.N. through Grant DE-AC02-98CH10886.

References and Notes

(1) Sutin, N. *Prog. Inorg. Chem.* **1983**, *30*, 441–498.
(2) Newton, M. D.; Sutin, N. *Annu. Rev. Phys. Chem.* **1984**, *35*, 437–480.
(3) Marcus, R. A.; Sutin, N. *Biochim. Biophys. Acta* **1985**, *811*, 265–322.
(4) Hush, N. S. *Prog. Inorg. Chem.* **1967**, *8*, 391–444.
(5) Jortner, J.; Bixon, M. *Adv. Chem. Phys.* **1999**, *106 and 107*, . entire volumes.
(6) Bixon, M.; Jortner, J. *Adv. Chem. Phys.* **1999**, *106*, 35–202.
(7) *Electron Transfer in Chemistry*; Balzani, V., Ed.; Wiley-VCH: New York, 2001.
(8) Newton, M. D. In *Electron Transfer in Chemistry* (see ref. 7); Piotrowiak, P., Ed.; Wiley-VCH Verlag GmbH: Weinhein, Germany, 2001; Vol *1*; Principles, Theories, Methods and Techniques, p3−63.
(9) Davis, W. B.; Svec, W. A.; Ratner, M. A.; Wasielewski, M. R. *Nature* **1997**, *396*, 60.
(10) Lewis, F. D.; Zhu, H. H.; Daublain, P.; Fiebig, T.; Raytchev, M.; Wang, Q.; Shafirovich, V. *J. Am. Chem. Soc.* **2006**, *128*, 791–800.
(11) Rosokha, S. V.; Kochi, J. K. *Acc. Chem. Res.* **2008**, *41*, 641–653.
(12) Creutz, C.; Newton, M. D.; Sutin, N. *J. Photochem. Photobiol. A* **1994**, *82*, 47–59.
(13) Newton, M. D. *Chem. Rev.* **1991**, *91*, 767–792.
(14) Skourtis, S. S.; Beratan, D. N. *Adv. Chem. Phys.* **1999**, *106*, 377–452.
(15) Stuchebrukhov, A. A. *Theor. Chem. Acc.* **2003**, *110*, 291–306.
(16) Evenson, J. W.; Karplus, M. *J. Chem. Phys.* **1992**, *96*, 5272–5278.
(17) Ratner, M. A. *J. Phys. Chem.* **1990**, *94*, 4877–4883.
(18) Voityuk, A. A. *J. Phys. Chem. B* **2005**, *109*, 17917–17921.
(19) Voityuk, A. A. *J. Chem. Phys.* **2006**, *124*, 064505.
(20) Lambert, C.; Amthor, S.; Schelter, J. *J. Phys. Chem. A* **2004**, *108*, 6474–6486.
(21) Amthor, S.; Lambert, C.; Dummler, S.; Fischer, I.; Schelter, J. *J. Phys. Chem. A* **2006**, *110*, 5204–5214.
(22) Nelsen, S. F.; Weaver, M. N.; Luo, Y.; Lockard, J. V.; Zink, J. I. *Chem. Phys.* **2006**, *324*, 195–201.
(23) Brunschwig, B. S.; Creutz, C.; Sutin, N. *Chem. Soc. Rev.* **2002**, *31*, 168–184.
(24) Cave, R. J.; Newton, M. D.; Kumar, K.; Zimmt, M. B. *J. Phys. Chem.* **1995**, *99*, 17501–17504.
(25) Rust, M.; Lappe, J.; Cave, R. J. *J. Phys. Chem. A* **2002**, *106*, 3930–3940.
(26) Mulliken, R. S. *J. Am. Chem. Soc.* **1950**, *72*, 600–608.
(27) Forster, T. In *The Exciplex*; Gordon, M., Ware, W. R., Eds.; Academic Press: New York, 1975; p 1.
(28) Bixon, M.; Jortner, J.; Verhoeven, J. W. *J. Am. Chem. Soc.* **1994**, *116*, 7349.
(29) Gould, I. R.; Young, R. H.; Mueller, L. J.; Albrecht, A. C.; Farid, S. *J. Am. Chem. Soc.* **1994**, *116*, 8188–8199.
(30) Murrell, J. N. *J. Am. Chem. Soc.* **1959**, *81*, 5037–5043.
(31) Cave, R. J.; Newton, M. D. *J. Chem. Phys.* **1997**, *106*, 9213–9226.
(32) McConnell, H. M. *J. Chem. Phys.* **1961**, *35*, 508.
(33) Pheasant, S.; Kouzelos, J. A.; Van Ryswyk, H.; Cave, R. J. *Mol. Simul.* **2006**, *32*, 677–693.
(34) Voityuk, A. A. *Chem. Phys. Lett.* **2006**, *422*, 15–19.
(35) Katz, D. J.; Stuchebrukhov, A. A. *J. Chem. Phys.* **1998**, *109*, 4960–4970.
(36) Newton, M. D. *Theor. Chem. Acc.* **2003**, *110*, 307–321.
(37) Lappe, J.; Cave, R. J.; Newton, M. D.; Rostov, I. V. *J. Phys. Chem. B* **2005**, *109*, 6610–6619.
(38) Newton, M. D. *Isr. J. Chem.* **2004**, *44*, 83.
(39) Newton, M. In *Continuum Solvation Models in Chemical Physics: From Theory to Applications*Mennucci, B., Cammi, R., Eds.; John Wiley & Sons, Ltd: New York, 2007; pp 389−413.
(40) Newton, M. D.; Ohta, K.; Zhong, E. *J. Phys. Chem.* **1991**, *95*, 2317–2326.
(41) Curtis, L. A.; Naleway, C. A.; Miller, H. R. *Chem. Phys.* **1993**, *176*, 387.
(42) Shephard, M. J.; Paddon-Row, M. N.; Jordan, K. D. *Chem. Phys.* **1993**, *176*.
(43) Senthilkumar, K.; Grozema, F. C.; Guerra, C. F.; Bickelhaupt, F. M.; Lewis, F. D.; Berlin, Y. A.; Ratner, M. A.; Siebbeles, L. D. A. *J. Am. Chem. Soc.* **2005**, *127*, 14894–14903.
(44) Paddon-Row, M. N.; Wong, S. S.; Jordan, K. D. *J. Chem. Soc., Perkin Trans. 2* **1990**, 425–430.
(45) Liang, C. X.; Newton, M. D. *J. Phys. Chem.* **1992**, *96*, 2855–2866.
(46) Cave, R. J.; Newton, M. D. *Chem. Phys. Lett.* **1996**, *249*, 15.
(47) Newton, M. D.; Cave, R. J. In *Molecular Electronics*; Ratner, M. A., Jortner, J., Eds.; Blackwell: Oxford, UK, 1997; pp 73−118.
(48) Lowdin, P.-O. *J. Chem. Phys.* **1950**, *18*, 365.
(49) Newton, M. D. *Coord. Chem. Rev.* **2003**, *238*, 167–185.
(50) Pacher, T.; Koppel, H.; Cederbaum, L. S. *J. Chem. Phys.* **1991**, *95*, 6668–6680.
(51) Logan, J.; Newton, M. D. *J. Chem. Phys.* **1983**, *78*, 4086–4091.
(52) Newton, M. D. *J. Phys. Chem.* **1988**, *92*, 3049–3056.
(53) Farazdel, A.; Dupuis, M.; Clementi, E.; Aviram, A. *J. Am. Chem. Soc.* **1990**, *112*, 4206–4214.
(54) Zhang, L. Y.; Friesner, R. A.; Murphy, R. B. *J. Chem. Phys.* **1997**, *107*, 450–459.
(55) Oh, D. H.; Sano, M.; Boxer, S. G. *J. Am. Chem. Soc.* **1991**, *113*, 6880–6890.
(56) Brunschwig, B. S.; Creutz, C.; Sutin, N. *Coord. Chem. Rev.* **1998**, *177*, 61–79.
(57) Onuchic, J. N.; Beratan, D. N.; Hopfield, J. J. *J. Phys. Chem.* **1986**, *90*, 3707.
(58) Liang, C. X.; Newton, M. D. *J. Phys. Chem.* **1993**, *97*, 3199–3211.
(59) Robin, M. B.; Day, P. *Adv. Inorg. Chem. Radiochem.* **1967**, *10*, 247.
(60) Subotnik, J. E.; Yeganeh, S.; Cave, R. J.; Ratner, M. A. *J. Chem. Phys.* **2008**, *129*, 244101.
(61) Subotnik, J. E.; Cave, R. J.; Steele, R. P.; Shenvi, N. *J. Chem. Phys.* **2009**, *130*, 234102.
(62) Orlandi, G.; Siebrand, W. *J. Chem. Phys.* **1973**, *58*, 4513–4523.
(63) Reimers, J. R.; Hush, N. S.; Sammeth, D. M.; Callis, P. R. *Chem. Phys. Lett.* **1990**, *169*, 622–626.
(64) Reimers, J. R.; Hush, N. S. *Chem. Phys.* **1990**, *146*, 105–114.
(65) Creutz, C.; Taube, H. *J. Am. Chem. Soc.* **1969**, *91*, 3988–9.
(66) Creutz, C.; Taube, H. *J. Am. Chem. Soc.* **1973**, *95*, 1096.
(67) Brown, G. M.; Hopf, F. R.; Meyer, T. J.; Whitten, D. G. *J. Am. Chem. Soc.* **1975**, *97*, 5385–5390.
(68) Becke, A. D. *J. Chem. Phys.* **1993**, *98*, 5648–5652.
(69) Hay, P. J.; Wadt, W. R. *J. Chem. Phys.* **1985**, *82*, 270–283.
(70) Dunning, T. H. *J. Chem. Phys.* **1970**, *53*, 2823.
(71) Furholz, U.; Burgi, H. B.; Wagner, F. E.; Stebler, A.; Ammeter, J. H.; Krausz, E.; Clark, R. J. H.; Stead, M. J.; Ludi, A. *J. Am. Chem. Soc.* **1984**, *106*, 121–123.
(72) Demadis, K. D.; Hartshorn, C. M.; Meyer, T. J. *Chem. Rev.* **2001**, *101*, 2655–2686.
(73) Rocha, R. C.; Rein, F. N.; Jude, H.; Shreve, A. P.; Concepcion, J. J.; Meyer, T. J. *Angew. Chem., Int. Ed.* **2008**, *47*, 503–506.
(74) Kohn, W.; Sham, L. J. *Phys. Rev.* **1965**, *140*, 1133.
(75) Koopmanns, T. *Physica A (Amsterdam)* **1933**, *1*, 104.
(76) Zhang, L. T.; Ko, J.; Ondrechen, M. J. *J. Am. Chem. Soc.* **1987**, *109*, 1666–1671.
(77) Bencini, A.; Ciofini, I.; Daul, C. A.; Ferretti, A. *J. Am. Chem. Soc.* **1999**, *121*, 11418–11424.
(78) Reimers, J. R.; Cai, Z. L.; Hush, N. S. *Chem. Phys.* **2005**, *319*, 39–51.
(79) Reimers, J. R.; Hush, N. S. *Chem. Phys.* **1996**, *208*, 177–193.
(80) Coropceanu, V.; Boldyrev, S. I.; Risko, C.; Bredas, J. L. *Chem. Phys.* **2006**, *326*, 107–114.
(81) Landau, L. *Phys. Z. Sowjet.* **1932**, *2*, 46.
(82) Zener, C. *Proc. R. Soc., Ser. A* **1932**, *137*, 696.
(83) Creutz, C.; Chou, M. H. *Inorg. Chem.* **1987**, *26*, 2995–3000.
(84) Pearl, G. M.; Zerner, M. C. *J. Am. Chem. Soc.* **1999**, *121*, 399–404.

JP102353Q